ESRF	**Experiment title:** **Exploring the competition of antiferrodistorsive and polar instabilities in $Sr_{1-x}Ba_xTiO_3$ system using X-ray Powder Diffraction and Pair Distribution Function**	**Experiment number**: **HC-2946**
Beamline: ID22	**Date of experiment**: from: 15/07/2017 to: 22/07/2017	**Date of report**: 27.02.2020
Shifts: 18	**Local contact(s)**: CODURI Mauro	*Received at ESRF:*

Names and affiliations of applicants (* indicates experimentalists):

Marco Scavini*, Stefano Checchia*, Davide Balestra*
Università degli Studi di Milano, Dip. di Chimica, Milano, Italy;

Mauro Coduri*, ESRF, Grenoble, France

Serena Chiara Tarantino, Università degli Studi di Pavia, Dip. di Scienze della Terra, Pavia, Italy;

Report

Introduction

Titanates ($ATiO_3$), a class of perovskite compounds attracting much fundamental and applied science, distort from the parent cubic structure (s.g. *Pm*-3*m*) decreasing their symmetry due to different phonon instabilities. Many of these transitions are influenced by steric effects, generally expressed by the tolerance factor (Goldschmidt) $t=(r_A+r_O)/\sqrt{2}(r_B+r_O)$, where r_A, r_B and r_O are the ionic radii of cations in the A, B and oxygen sites, respectively.

For small A cations $t<1$; the system tends to have strong antiferrodistortive (AFD) octahedral-tilting instabilities such as in $CaTiO_3$ (CTO, $t=0.946$) causing the symmetry lowering to the centrosymmetric *I*4*/mcm* space group at 1635 K.[1] Conversely, zone-center ferroelectric (FE) modes should be stronger in perovskites with $t>1$. $BaTiO_3$ (BTO, $t=1.063$), a typical example of the emergence of spontaneous electric polarization, undergoes a series of phase transitions on cooling (*Pm*-3*m* → *P*4*mm* → *Amm*2 → *R*3*m*) related to zone-center polar instability [2], involving the FE displacement of Ti.

$SrTiO_3$ (STO, $t=1.002$), is unstable to both FE (Γ-point) and AFD (R-point) phonons.[3] It is well known, however, that quantum fluctuations prevent condensation of the FE mode down to zero temperature [4]. Thus, the STO phase diagram was interpreted in terms of competition between the polar and the antiferrodistorsive instabilities [5], whereby the FE instability should be progressively suppressed by a stronger octahedral-tilting instability.

The interplay between STO structure and FE instability has been recently reexamined [5] : by computing the energy gain due to FE as a function of octahedral tilt angle (ϕ), it was found that the TiO_6 rotation indeed dampens the FE mode, but only for small ϕ angles. Larger ϕ angles (>6°) combined with increased tetragonality do in fact enhance the FE distortion in order to recover the loss of Ti-O π bonding along the *c* axis

We confirmed this assumption experimentally by investigating the structure of Pr-doped $Sr_{1-x}Pr_xTiO_3$ (SPTO) [6]. By substituting Sr^{2+} with the smaller Pr^{3+} ion we lowered the $SrTiO_3$ tolerance factor, boosting both the tilting angle and the AFD transition temperature; but at the same time FE structural responses were switched on, such as hard polar Raman modes and a polarization-induced electrostrictive strain. In addition, our PDF analysis

evidenced local AFD distortions much larger than in the long-range AFD structure and locally non-zero ϕ values even within average cubic phases [6], in agreement with the DFT results in Ref. [5].

The aim of the present experiment was to investigate the cooperation/competition of FE and AFD instabilities in STO based solid solutions with $t>1$ This was done doping $SrTiO_3$ with small concentrations of Ba ($\leq 35\%$). Forming $Sr_{1-x}Ba_xTiO_3$ (SBTO) solid solutions and investigating the structure at temperatures between 10 and 300 K

We measured accurately the structure of SBTO as a function of both temperature and composition, by means of high resolution powder diffraction measurements coupled with the real-space Pair Distribution Function (PDF) analysis.

Samples

Samples of $Sr_{1-x}Ba_xTiO_3$ (x = 0.025, 0.05, 0.075, 0.10, 0.15, 0.20, 0.25, 0.30 and 0.35) were prepared by using solid state synthesis. Stoichiometric mixtures of $SrCO_3$ (Aldrich, 99.9%), $BaCO_3$ (99.9%), TiO_2 (99.9%) were mixed and underwent firing cycles at1000 °C, 1200 °C, 1200 °C, 1400°C with intermediate grindings.

Data collection strategy

XRPD data were collected at the ID22 beamline selecting an X-ray wavelength of λ = 0.399946 Å and using a 9-elements detector array (high resolution setup). Powdered samples of SBTO were put in 0.3 mm capillaries and cooled down to 10 K in a He-cryostat; data were collected up to 100 K. Measurements between 90 and 300 K were carried out using the cryostream of ID22.

Rietveld quality XRPD patterns were collected up to $Q_{max}\approx 12$ Å^{-1} at 12, 25, 40, 60, 80, 90, 100, 120, 150, 200, 250, 300 K. Measurements at 90 and 100 K were collected twice, using both the crysostream and the cryostat to reveal possible T mismatches. PDF quality HR-XRPD measurements have been collected on x=0.10, 0.25 and 0.35 samples at 90 K. Data up to Q_{max} 27.5 Å^{-1} were fast Fourier transformed after data reduction to get the G(r) functions

For additional PDF quality XRPD measurements on all the samples at 90 K we used the area detector of ID22 (λ=0.1771 Å, Q_{max}= 28.5 Å^{-1}).

Results:

All solid solution members are cubic down to 10 K. The cell volume expands on raising x. In Figure 1 the Rietveld refinement of the samples x = 0.30 and T= 10 K using the cubic perovskite structural model (space group *Pm*-3*m*) is shown as an examples.

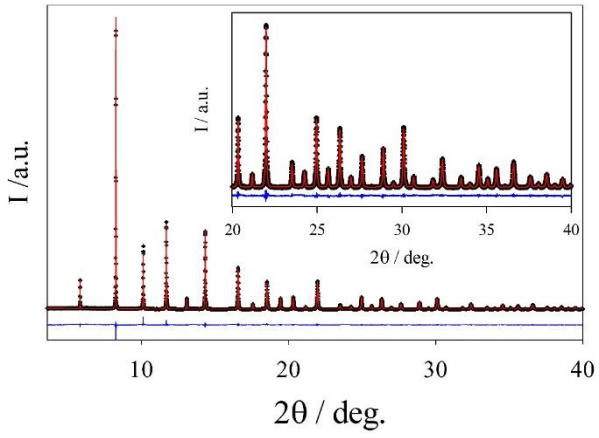

Figure 1. Rietveld refinements of XRPD patterns collected at 10 K on on x=0.30 sample using the cubic *Pm*-3*m* model. Experimental data (black symbols) are shown together with the fit (red curve) and the residuals (blue curve).

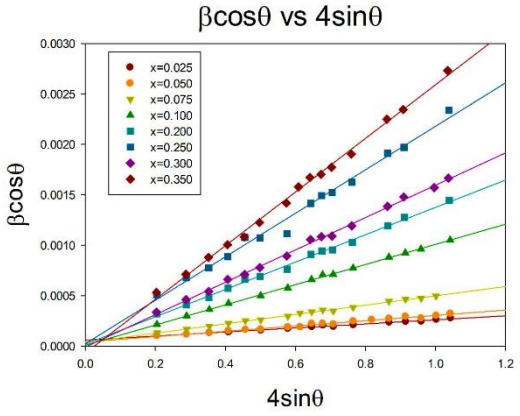

Figure 2. Williamson Hall plots calculated on data collected at 300 K on all the samples. The slope of the βcosθ va 4sinθ plot is the micro-strain parameter ε

At the same time the Williamson-Hall size and strain analysis of data collected at 300 K revealed a micrometric crystallite size for all the sample and an almost linear increase of the micro-strain parameters ε (= Δ*a*/*a*)) on increasing *x*.

Figure 2 displays the W.-H. plots: βcosθ vs 4sinθ, where *β* are the peaks integral breadth values. For x=0.35, ε takes a value as large as ≈ 0.0037 suggesting huge disorder at the mesoscopic range.

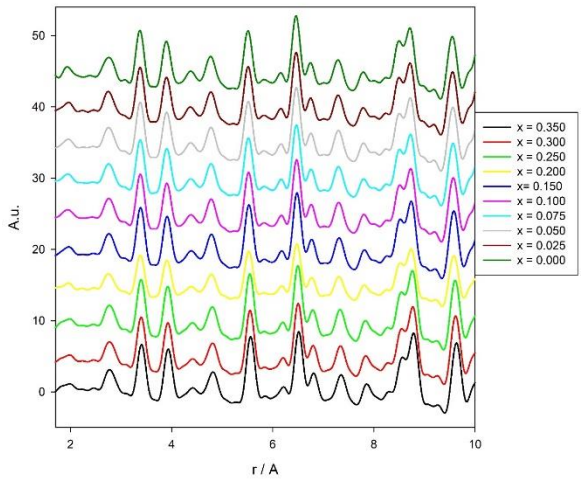

Figure 3.

Short range parts of the G(r) functions collected at 90 K on all the samples

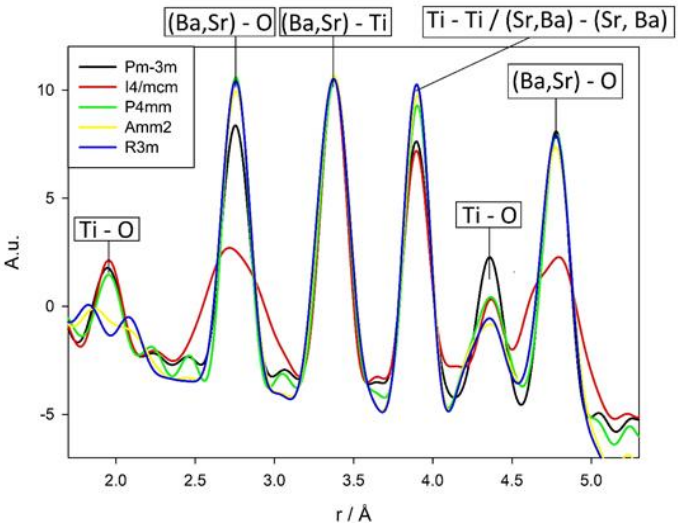

Figure 4. Calculated G(r) using the cubic Pm-3m structure, the I4/mcm low T AFD structure of STO and the three polar structures of BTO (*P*4*mm*, *Amm*2 and *R*3*m* on lowering *T*). Labels indicate the couples of atoms involved in each peak

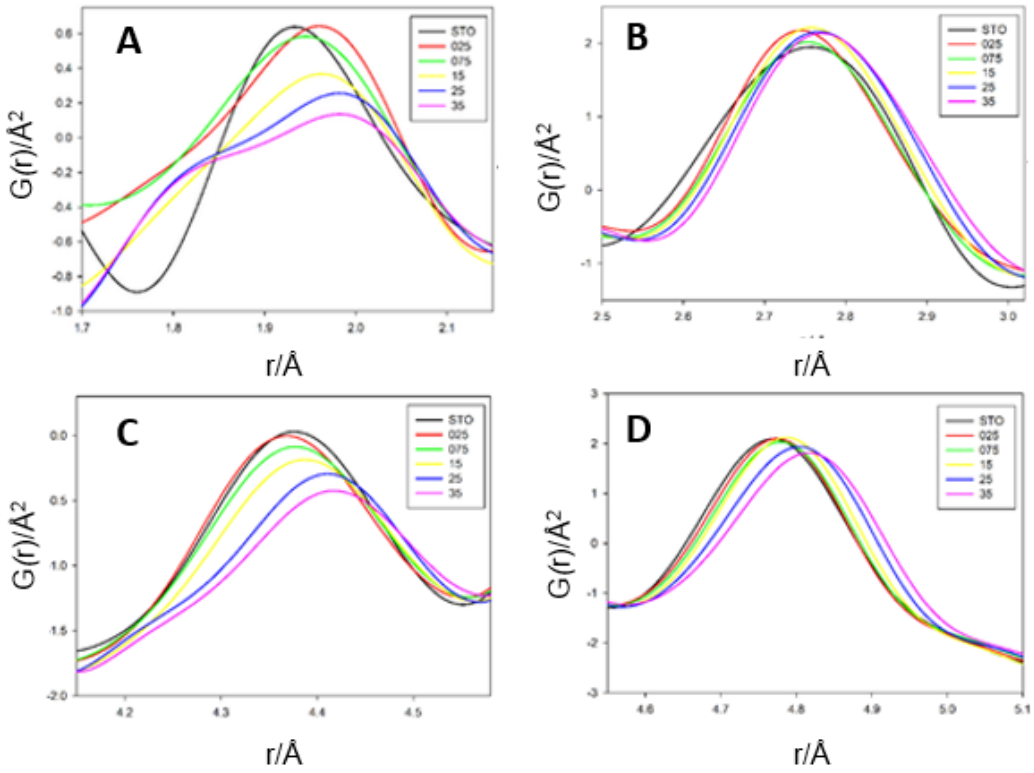

Figure 6. Experimental G(r) peaks corresponding to the NN Ti-O (A), Sr/Ba-O (B), next NN Ti-O (C) and Sr/Ba-O (D) distances.

The short- and medium-range structures have been studied by means of PDF analysis through the G(*r*) function. Analysing G(*r*) curves for different compositions in a wide range of interatomic distances r allows

understanding both nature and coherence length of distortions induced by the different chemical environments of Ba and Sr.

In Figure 3 the short range parts of the G(r) functions collected at 90 K on all the samples are reported.

G(r) functions up to 5 Å) were analysed by the direct analysis of peaks using Gaussian functions. In fact, on the one hand, perovskite structure allows labelling each peak with the couple of atoms involved (in case of solid solutions Sr and Ba share the same peaks), as shown in Fig. 4; on the other hand, symmetry breaks brings to broadening or even splitting of selected peaks. In particular, AFD tilting of TiO_6 octahedra (i.e. the low *T* structure of STO, space group *I*4/*mcm*) broadens the Sr/Ba-O peaks (2nd and 6th peaks in Fig.4), while Ti-O peaks broaden preferentially in case of FE distortions (1st and 5th peaks in Fig. 4).

In Figure 5 ~~are~~ reports portions of selected experimental G(r) functions corresponding to the NN Ti-O (A) and Sr/Ba-O (B) distances as well as the next NN Ti-O (C) and Sr/Ba-O (D) ones. The Ti-O peaks broaden and split into two, as predicted by *R*-3*m* and *Amm*2 models; conversely, the NN and next NN Sr/Ba-O peak remains unaffected by doping; only the position of their maxima shifts toward larger r values, probably due to the larger ionic radius of Ba with respect to Sr. This analysis points to a progressive FE structural distortion on Ba doping.

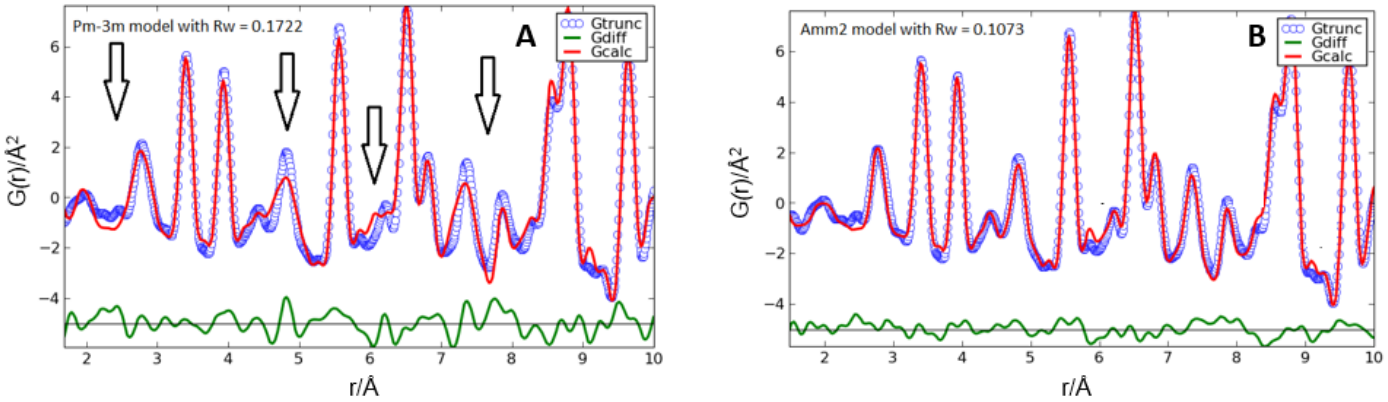

Figure 7. Real space Rietveld analysis of $G(r)_{x=0.35}$ using either the cubic *Pm*-3*m* (left side panel) or the Amm2 (right side panel) models. Experimental data (circles) are shown together with the fit (red curves) and the residuals (red curves). Arrows indicate *r* zones where the cubic model fails.

The same eperimental G(r) functions have been fitted against the above described structuarl models, using the so called Real Space Rietveld analysis as implemented in PDFGui suite of programs.

In all cases, bad fits are obtained using the cubic model. On increasing *x*, the best fits are observed applying the polar *Amm*2 model. In figure 7 are shown as an example, the fits of $G(r)_{x=0.35}$ using the cubic *Pm*-3*m* and the orthorhombic polar *Amm*2 models. The latter model brings to a clear improvement of the fit quality e.g. in the zones 2-3 and 4-5 Å where Ti-O and Sr/Ba-O distances drop. So, we can safely affirm that in SBTO solid solution the structure display FE distorsions at the local scale.

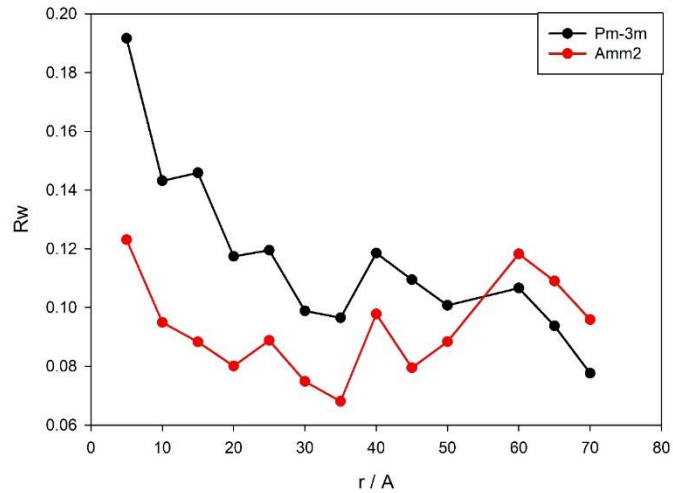

Figure 8

Residuals of box car refinements (10 Å wide *r* ranges) of $G(r)_{x=025}$ functions using *Pm*-3*m* and *Amm*2 models. r values are the cenroids of the refinement ranges.

To reconcile the local scale symmetry decrease with the cubic average structure, real space refinements have been applied to larger r values using experimental G(r) functions obtained by High Resolution data using a box car refinement strategy (10 Å wide intervals). The residuals of fits of the $G(r)_{x=0.25}$ data using either the *Pm*-3*m* or *Amm*2 models are shown in Figure 8. r value are the centroids of each interval. At low *r* values, the fit quality using *Amm*2 model is much better than the cubic case. However, the difference start decreasing and the two models supply equivalent fits around 5-6 nm. This suggests that coherently distorted zones are few nanometers wide (poler nano-regions) and they merge to the cubic structure at lagger *r* values.

The emerging scenario is that local polar distortions exist in the SBTO solid solutions and their coherence length depends on the Ba concentration and distribution. The growing polar nanodomains grow up oriented randomly, frustrating their long range ordering and bringing to a cubic structure on average, at least for $x \leq 0.35$.

Outlooks and future developments

The high *Q*-resolution of the ID22 beamline made it possible to study the structure of SBTO solid solutions at different length scales, which is of extreme importance to fully understand the structural evolution of locally distorted regions into polar nano-regions.

Since BTO undergoes three different structural phase transitions (*Pm*-3*m* → *P*4*mm* → *Amm*2 → *R*3*m* on cooling), it is worth supposing that they (or some of them) could be observed also in SBTO solid solutions by extending measurements toward larger Ba concentrations.

We will propose a new experiment aimed at completing the phase diagram of $Sr_{1-x}Ba_xTiO_3$ system, extending high resolution XRPD measurements to the $0.35<x<1$ compositional range. PDF quality measurements will be carried out at 90 K; the HR setup will allow observing G(*r*) amplitudes at *r* values up to the range of teens of nanometers. In this way, it will be possible to reveal whether long range phase transition are driven by the percolation of distorted domains or by some more subtle mechanism as in the case of Pr-doped STO.

Parallel to the diffraction investigation, the same group of proponent is carrying out also Raman measurements and ab-initio (DFT) calculations on the same compositions.

References

[1] W. Zhong, D. Vanderbilt, Phys. Rev. Lett., 74 (1995) 2587.

[2] J. F. Scott, Rev. Mod. Phys. 46 (1974) 83.

[3] M. Yashima, R. Ali, Solid State Ionics 180 (2009) 120-126.

[4] K.A. Muller, H. Burkard, Phys. Rev. B19 (1979) 3593.

[5] A. Aschauer, N.A. Spaldin, J. Phys.: Condens. Matter, 26 (2014) 122203.

[6] S. Checchia et al., Phys. Rev. B, 94 (2016) 104201 1-8